PHYSICAL REVIEW D **91,** 054015 (2015)

Relic neutralino surface at a 100 TeV collider

Joseph Bramante,[1] Patrick J. Fox,[2] Adam Martin,[1] Bryan Ostdiek,[1] Tilman Plehn,[3] Torben Schell,[3] and Michihisa Takeuchi[4]

[1]*Department of Physics, University of Notre Dame, Notre Dame, Indiana 46556, USA*
[2]*Theoretical Physics Department, Fermilab, Batavia, Illinois 60510, USA*
[3]*Institut für Theoretische Physik, Universität Heidelberg, Germany*
[4]*Kavli IPMU (WPI), The University of Tokyo, Kashiwa, Japan*

(Received 23 December 2014; published 11 March 2015)

We map the parameter space for minimal supersymmetric Standard Model neutralino dark matter which freezes out to the observed relic abundance, in the limit that all superpartners except the neutralinos and charginos are decoupled. In this space of relic neutralinos, we show the dominant dark matter annihilation modes, the mass splittings among the electroweakinos, direct detection rates, and collider cross sections. The mass difference between the dark matter and the next-to-lightest neutral and charged states is typically much less than electroweak gauge boson masses. With these small mass differences, the relic neutralino surface is accessible to a future 100 TeV hadron collider, which can discover interneutralino mass splittings down to 1 GeV and thermal relic dark matter neutralino masses up to 1.5 TeV with a few inverse attobarns of luminosity. This coverage is a direct consequence of the increased collider energy: in the Standard Model events with missing transverse momentum in the TeV range have mostly hard electroweak radiation, distinct from the soft radiation shed in compressed electroweakino decays. We exploit this kinematic feature in final states including photons and leptons, tailored to the 100 TeV collider environment.

DOI: 10.1103/PhysRevD.91.054015 PACS numbers: 14.80.Nb, 12.60.-i, 95.35.+d

I. INTRODUCTION

Understanding the properties of dark matter is a next major step in experimental and theoretical particle physics [1]. In this paper we will establish that a 100 TeV collider provides excellent prospects for detecting weakly interacting dark matter. In addition, we show that a 100 TeV collider can expose nearby states that interact with the dark matter.

Many scenarios of physics beyond the Standard Model predict that dark matter is the lightest particle charged under a stabilizing symmetry, and that it freezes out during the radiation-dominated expansion of the Universe. In this paper we focus on the neutralino and chargino sector of the minimal supersymmetric Standard Model (MSSM), where the lightest neutralino freezes out to the observed relic abundance. We refer to the four neutralinos and the two charginos of the MSSM collectively as electroweakinos, and the lightest neutralino as the lightest supersymmetric particle (LSP). Over the supersymmetric parameter space this Majorana fermion can be a mixture of the neutral components of a triplet under $SU(2)_L$ (a wino), a singlet (a bino), or two $SU(2)_L$ doublets (higgsinos). If the supersymmetric mass parameters of the electroweakinos are well separated, intermultiplet mixing can be neglected and the lightest neutralino can be studied as a pure state: pure singlet, triplet, or doublet, depending on which supersymmetric mass parameter is lowest. However, once we apply LEP, LHC, and astrophysical constraints, the only pure state possibility that can fit the required relic abundance is pure higgsino [2–5]. There is much more viable parameter space if we give up the pure state hypothesis and allow the lightest neutralino to be an admixture of bino, wino, and higgsino, so-called well tempering [6]. In both the pure higgsino and well-tempered scenarios, there are additional neutralino and chargino states that have similar mass to the LSP. These states play an important role in establishing the observed dark matter density, and they will be crucial to the collider studies proposed here.

While the electroweakino sector of the MSSM is just one example of a dark matter framework, the existence of other nearby (in mass) states that communicate with the dark matter at the renormalizable level can be argued from fairly general grounds. To understand why, let us assume dark matter is a thermal relic and has some nongravitational interactions with the Standard Model. The partial wave amplitude unitarity bound in Ref. [7] implies that any dark matter populating the Universe through the classic freeze-out mechanism is lighter than 340 TeV, so we can break up the models of dark matter into two groups: $m_\chi < 340$ TeV and $m_\chi > 340$ TeV, where m_χ is the mass of the dark matter agent.

For dark matter lighter than 340 TeV, the weakly interacting massive particle (WIMP) and WIMP-less miracles [8–11] emphasize that if the correct dark relic abundance is attained through freeze-out via a single mediator, then

$$\Omega_D h^2 = \frac{1}{\langle \sigma_a v \rangle} = \frac{m_D^2}{g_D^4} \simeq \frac{1}{\text{picobarn}}, \tag{1}$$

where (m_D, g_D) are the mass and the coupling associated with dark matter's thermal annihilation cross section, $\langle \sigma_a v \rangle$.

However, direct detection experiments constrain both spin-independent and spin-dependent dark matter cross sections with Standard Model particles to be well below a picobarn for dark matter masses less than 100 TeV [12–16]. Altogether, this implies that either a new mass state mediates dark matter freeze-out or a nearby mass state allows for nonstandard dark matter annihilation.[1]

For dark matter heavier than 340 TeV a viable relic abundance can still be achieved if the dark matter mass lies near a cross-section pole (e.g. dark matter exactly half the mass of a new s-channel mediator) or if it lies below nearly mass-degenerate states that induce additional, coannihilation interactions [21]. In both of these cases, the lightest mass eigenstate would normally overpopulate the primordial relic abundance, but instead annihilates to the observed abundance as a result of other states in the thermal bath.

The necessity of such an extended dark matter "sector," rather than a single dark matter particle, makes resolving dark matter mass splitting vital in parsing the physical implications of a detection of dark matter, wherever it occurs. In particular for collider searches this emphasizes the need to resolve nearby states, $O(10\%)$ heavier than the primary dark relic.

The existence of an extended dark sector is certainly true in minimal supersymmetric models where the lightest neutralino is the LSP and a cosmologically viable relic abundance is achieved. The neutralino LSP is always accompanied by some similar-mass states, usually within $\mathcal{O}(10\%)$ of the LSP mass, allowing for coannihilation during freeze-out. This happens both in constrained models [22–29] and the full MSSM [22,30–35], though exactly which states are nearby can vary greatly. Sleptons, squark, or charginos are all possibilities [36–44]. Squarks are far easier to produce at hadron colliders than electroweak particles, and are more strongly constrained by LHC limits. Sleptons are also fairly constrained due to their clean decay signal. The most difficult scenario to detect, and thus the focus of our work, is where the dark sector is purely composed of the electroweakinos (mass 0.2–3 TeV) and all other supersymmetric particles have been decoupled ($\gtrsim$10 TeV).

In addition to being difficult to constrain at the LHC, the interactions between electroweakino sector dark matter and nuclei are often extremely suppressed. Limits on the spin-dependent scattering of WIMPs [16,45–47] and indirect searches for MSSM electroweakino annihilation in the sun [48,49] at best constrain dark matter spin-dependent nucleon scattering to be less than 10^{-40} cm^2, but as we will see, the spin-dependent cross section of relic electroweakino dark matter can be $\lesssim 10^{-45}$ cm^2. In addition, while limits on spin-independent scattering [12–15] bound the dark matter nucleon cross section to be smaller than 10^{-44} cm^2 for TeV-mass dark matter, Sec. II will show that relic bino-wino dark matter has blind spots where the (tree-level) spin-independent cross section is smaller than 10^{-50} cm^2. Indeed, it was recently shown at next-to-leading order that if a doublet, triplet, singlet-doublet, or doublet-triplet of $SU(2)_L$ is heavy compared to a typical direct detection momentum transfer, the absolute spin-independent scattering cross section of such a particle will be around 10^{-48} cm^2 [50–54].

For TeV-mass dark matter, this cross section is much smaller than the solar neutrino scattering cross section, which provides a major irreducible background for current xenon and semiconductor-based direct detection methods [55]. Future directional dark matter detection experiments may overcome the solar neutrino background by subtracting off the solar neutrino diurnal variation (Refs. [56–58]). But even assuming these directional methods advance to their full potential and we find dark matter in low momentum transfer regimes, this will only be a first step in illuminating the properties of dark matter. Multiple detector materials across a number of experiments [59–64] would be necessary to fully characterize even the mass of a WIMP [65–67]. This suggests that production of dark matter at a hadron collider will be essential in clarifying any findings of direct detection experiments. While a low momentum transfer detection of dark matter could occur before collider detection, exposing the structure of the dark sector will require collider input.

Altogether, future direct and indirect detection are likely to leave one well-motivated scenario for physics beyond the Standard Model largely untested, namely a Universe containing only a few weakly interacting fermions in the 0.2–4 TeV mass range. In fact, this scenario realized in split supersymmetry has been proposed as a parsimonious route to grand unified theory scale unification, albeit with a necessarily fine-tuned solution to the hierarchy problem [68–80]. Regardless of UV motivations, if dark matter is a relic neutralino, there are significant blind spots in electroweakino mass parameter space where spin-independent and spin-dependent scattering (through LSP coupling to the Higgs and Z) vanishes, as examined in Refs. [81–85]. We will see that most of the presently unplumbed pockets of this MSSM parameter space can be unmasked by 100 TeV collider searches.

Recently, there has been significant work motivating a 100 TeV collider [86–94] from a dark matter perspective [95–101]. Key analysis strategies are monojet searches, soft leptons, and disappearing tracks. For pure wino and pure higgsino dark matter in the MSSM, disappearing tracks are a promising search strategy as long as the mass differences between the lightest electroweakino states are perturbatively stable at the 200 MeV level. Mixed relic neutralinos with additional heavier states can be targeted with soft (tri) leptons [95]. Same-sign or opposite-sign dilepton searches and trilepton signatures have the potential to cover some neutralino parameter space, based on inclusive effective

[1]There are, of course, exceptions to the standard freeze-out scenario, e.g. freeze in [17] and asymmetric dark matter [18,19], and exceptions to constraints on dark matter–Standard Model cross sections, e.g. leptophilic dark matter [20].

mass and transverse momentum cuts [99]. The additional production of neutralinos and charginos in weak boson fusion [102] will be rate limited and will only minimally contribute to the discovery potential [97]. In this paper we add a lepton-photon decay signature, which targets electroweakino mass splittings above 1 GeV and covers similar parameter space as the disappearing tracks, but without their sensitivity to a tuned mass splitting.

Moreover, the existing studies of electroweakino production at a 100 TeV collider focus on pure electroweakino states and do not take cosmological aspects into account. In this work, we link electroweakino discovery prospects directly to cosmological relic abundance requirements. As a starting point, we survey MSSM neutralino dark matter mass parameters to 4 TeV and chart every combination thereof which freezes out to the correct relic dark matter abundance. Most of this parameter space surface of relic neutralinos is accessible at a 100 TeV hadron collider, making use of the production of slightly heavier electroweakinos and subsequent decays through emission of an off-shell $Z \to \ell^+\ell^-$ or a photon. As we will see, the combination of ~TeV of missing energy with low momenta (~5–50 GeV) photons and/or leptons provides a sharp signature at very high energy hadron colliders.

II. THE RELIC NEUTRALINO SURFACE

Neutralinos in the MSSM are mixed mass eigenstates of the partners of the hypercharge gauge boson, the $SU(2)_L$ gauge boson, and Higgs bosons. This means that, depending on their field content, the lightest mass eigenstate interpolates between different WIMP scenarios. We begin with an exploration of parameter space defined by the spectrum of Standard Model fields plus electroweakino fields, with the added requirement that the lightest neutral electroweakino forms the dark matter relic abundance by freezing out of the primordial thermal bath. We decouple all nonelectroweakino MSSM fields, i.e. the squarks, sleptons, and additional Higgs bosons. With these assumptions, we have four free parameters, the mass of the bino (M_1), the mass of the wino (M_2), the mass of the higgsinos (μ), and the ratio of the vacuum expectation values of the two Higgs fields ($\tan\beta$). After fixing $\tan\beta$ we will study where in this three-dimensional parameter space the lightest neutralino freezes out to the observed relic density, its spin-dependent and spin-independent nucleon cross sections, what the mass difference between the lightest and second lightest electroweakino is, and what the relevant 100 TeV hadron collider cross sections are. In particular, the absolute mass splitting between the LSP dark matter agent and the neutralino or chargino next-to-lightest supersymmetric particle (NLSP) will be relevant for the 100 TeV collider search strategy.

Assuming thermal freeze-out of the lightest neutralino, the relic abundance depends on the neutralino's mass, the annihilation cross section, and the mass of any nearly mass-degenerate coannihilating particles. If the LSP is a pure gauge eigenstate with a nontrivial $SU(2)_L$ representation, for instance the higgsino or the wino, these will need to have large masses to compensate for efficient annihilations depleting their number density during the radiation-dominated era. In the MSSM the masses of the lightest pure WIMP states have to exceed 1 TeV for the higgsino and 3 TeV for the wino. In contrast, the gauge singlet bino inefficiently annihilates and will overclose the Universe if its mass is above ~5 GeV. If the lightest mass eigenstate mixes binos, higgsinos, and winos, either through explicit fractions of the lightest mass eigenstate or if the lightest eigenstate coannihilates with heavier electroweakinos, the resultant relic neutralinos can yield the observed relic abundance for masses very different than in the case of pure neutralino gauge eigenstates.

To generate the relic neutralino surface shown in Figs. 1–4 we calculate MSSM masses using SUSPECT3

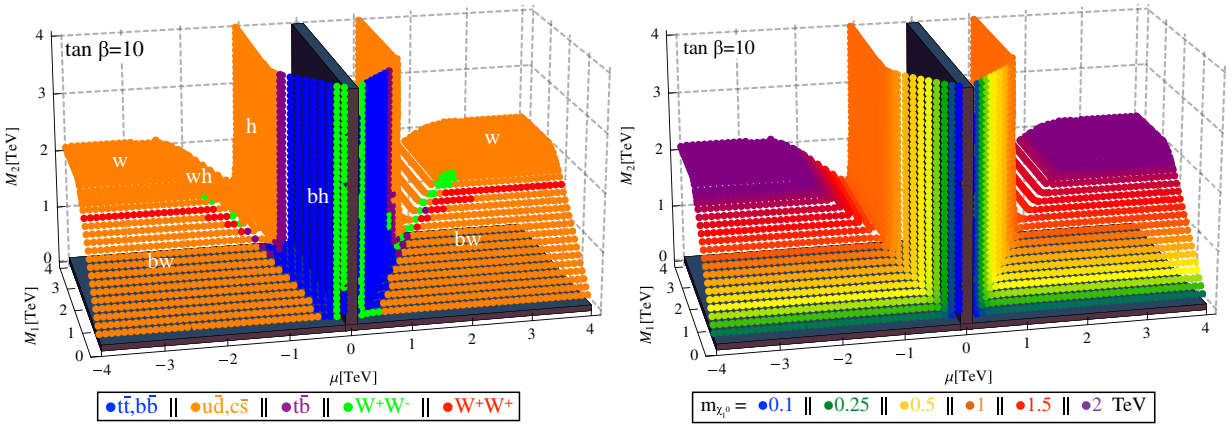

FIG. 1 (color online). (Left panel) Relic neutralino surface with the largest fraction of primordial annihilation products indicated by color. All points shown predict a dark matter relic density of $\Omega h^2 \simeq 0.12$. Regions ruled out by LEP constraints are occluded with a dark box. Planar surfaces of relic higgsinos, winos, bino-winos, bino-higgsinos, and wino-higgsinos are indicated with white letters. (Right panel) Mass of the lightest neutralino, the LSP, in TeV.

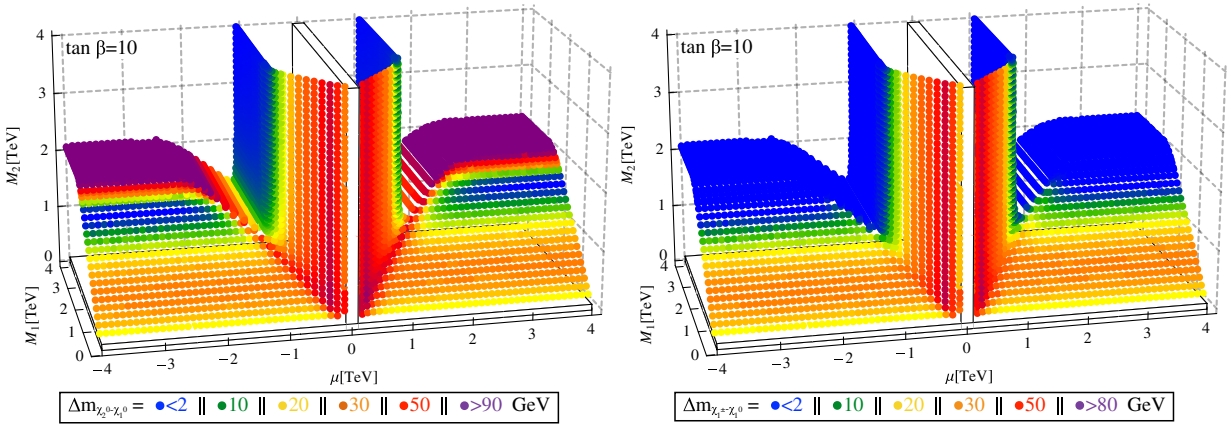

FIG. 2 (color online). Relic neutralino surface with mass splitting between χ_1^0 and χ_2^0 (left panel) and between χ_1^0 and $\chi_1^\pm$ (right panel) as indicated. Regions ruled out by LEP are occluded with a white box.

[103] and the frozen out relic abundance of the LSP using micrOMEGAs3 [104]. We do not include loop corrections to the neutralino masses, which are dominated by the scalar states, whose masses were set to 8 TeV, including the *CP*-odd Higgs [105–107]. Note that micrOMEGAs3 also calculates relic abundance at leading order. For most of the parameter space, after fixing the values of M_2 and μ, we vary M_1 until micrOMEGAs3 produces the correct relic abundance, $\Omega h^2 \simeq 0.12$. For parameter space where the relic abundance is attained with a decoupled bino, notably the wino-higgsino surface, we hold μ fixed and scan over M_2. Note that in Figs. 1–4 the SUSPECT3 and micrOMEGAs3 calculations were performed with the parameters M_1, M_2, and μ, defined at the decoupled scale (8 TeV) and β defined at m_Z. If $\tan\beta = 10$ at m_Z, this will run to $\tan\beta = 9.4$ at 8 TeV. We found that if instead all parameters are defined at m_Z the relic surface moves by no more than ∼10% in M_1, M_2, and μ.

We begin our journey across the relic neutralino surface with the relic wino. When $|\mu|$ and M_1 decouple, with values above 2 TeV, two plateaus at $M_2 = 2$ TeV correspond to pure wino dark matter with a mass around 2 TeV. For $\tan\beta = 10$ the features of the relic neutralino surface are almost perfectly symmetric around $\mu = 0$. The dominant annihilation channel for the pure wino is coannihilation with the close-by chargino through an off-shell W boson, subsequently decaying to light-flavor quarks. micrOMEGAs3 does not include the Sommerfeld enhancement [108–113] to wino annihilation, so this surface lies below the usual value of $M_2 \simeq 2.8$ TeV. (The relic higgsino mass, on the other hand, is unaltered by Sommerfeld annihilation enhancement [114].) Edges of the pure wino plateau fall off, at smaller M_1 and $|\mu|$ respectively, to sloped bino-wino and wino-higgsino surfaces, with either $M_1 \sim M_2$ or $M_2 \sim |\mu|$. On all of these surfaces coannihilation and mixing with the wino bolsters the annihilation of the lightest neutralino.

An amusing effect occurs on the bino-wino slope around $M_1 \sim M_2 \sim 1.7$ TeV, where the single largest annihilation channel is $\chi^\pm\chi^\pm \to W^\pm W^\pm$. Here, the mass difference between the lightest neutralino and the lightest chargino

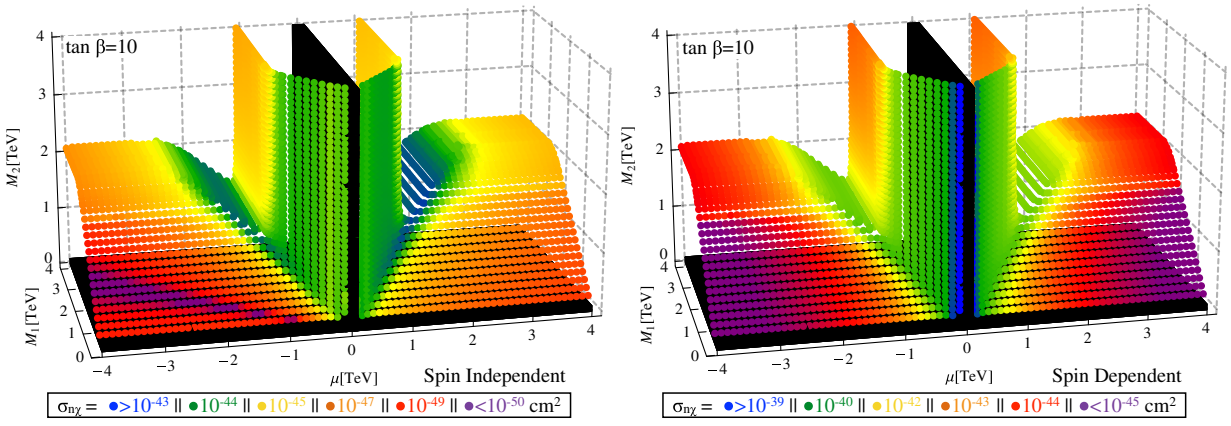

FIG. 3 (color online). Relic neutralino surface with spin-independent (left panel) and spin-dependent (right panel) scattering cross sections of the LSP on nucleon. At each point in each plot, the larger of the χ-proton and χ-neutron scattering cross sections is given.

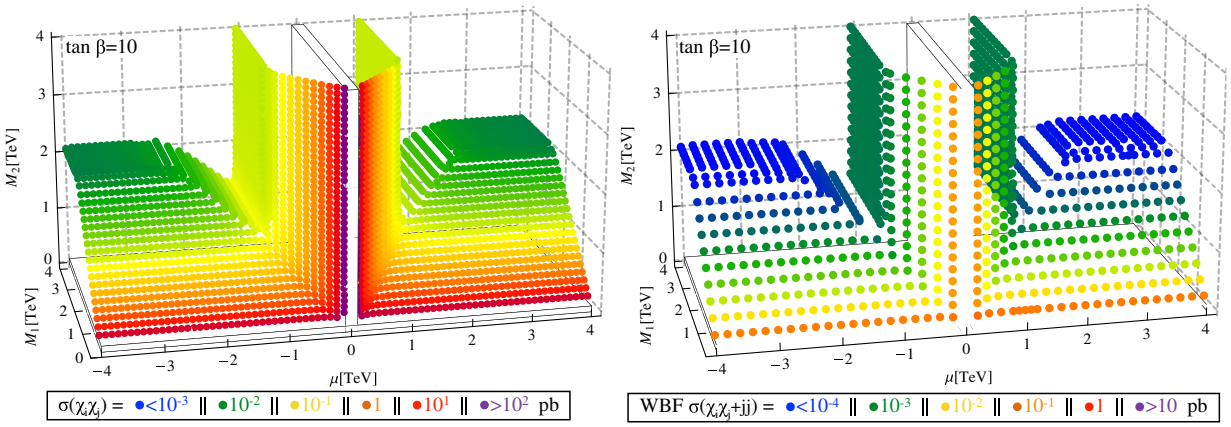

FIG. 4 (color online). Relic neutralino surface with cross sections for direct pair production $pp \to \chi\chi$ (left panel), and weak boson fusion pair production $pp \to \chi\chi jj$ (right panel), at 100 TeV collider energy. At each point, all contributions for all electroweakino final states are summed. Regions ruled out by LEP are occluded with a white box.

is so small that the main annihilation process leading to the observed dark matter relic density involves the chargino and not the actual LSP.

Starting from the pure wino plateaus, the mixed LSP wino-higgsino surface terminates in a valley against a sheet of pure higgsino relic dark matter at $|\mu| \simeq 1.1$ TeV. For such a pure higgsino, chargino coannihilation is again the leading dark matter annihilation process. On the diagonal $|\mu| \sim M_1 \sim M_2$ this valley opens onto a ridge at the intersection of the wino-higgsino, bino-wino, and eventually bino-higgsino surfaces. This ridge contains bino-wino-higgsino mixing with a dominant annihilation to W^+W^-, both through coannihilation with the second lightest neutralino and through a t-channel chargino with sizable couplings to the weak gauge bosons.

On the bino-higgsino slope, large values of $|\mu|$ imply large neutralino masses and hence an annihilation to heavy fermions $t\bar{t}$. Usually, this annihilation process proceeds through a heavy Higgs state in the s channel. Once we decouple the heavy Higgs states at 8 TeV the same role is played by the longitudinal modes of the Z boson. Towards smaller values of $|\mu|$ the available energy in the scattering process drops below the $t\bar{t}$ threshold and the main annihilation goes into W^+W^- pairs, again through a longitudinal Z in the s channel coupling to the higgsino components of the lightest neutralino.

Unlike a pure wino LSP and a pure higgsino LSP the relic neutralino surface does not feature a pure bino LSP, because in the absence of coannihilating scalars it would not be able to produce a relic density small enough to fit observation.

In models where the only low-energy part of the supersymmetric spectrum are the electroweakinos, the mass difference between the neutralino LSP and the second lightest neutralino and lightest chargino is crucial, not only for the dark matter (co)annihilation rate, but also for electroweakino decay signatures at colliders. From the discussion of Fig. 1 we know that chargino coannihilation is crucial to obtain the correct relic density. The typical mass splitting required for coannihilation is $\mathcal{O}(10\%)$ or less. In Fig. 2 we show the absolute mass difference between the LSP and the second lightest neutralino (left panel) and the lightest chargino (right panel). Over almost the entire parameter space the relative mass splitting stays below 5%, except for part of the diagonal bino-higgsino sheets. This confirms that coannihilation largely determines the structure of the relic neutralino surface.

For neutralino and chargino decays the absolute mass difference (GeV) is more relevant than the relative (percentage) mass difference, because it determines if a $1 \to 2$ particle decay can occur through an on-shell $W^\pm$ or Z boson. If on-shell decays are forbidden, decays must proceed through an off-shell weak gauge boson or a loop-induced decay.

For the mass difference between the lightest two neutralinos, we see that some of the pure wino regime will allow for an on-shell decay $\chi_2^0 \to \chi_1^0 Z$. This means that collider searches for pure winos can use leptonic Z decays, including a same-flavor opposite-sign Z-mass constraint [95,97,98]. This makes one 100 TeV hadron collider search strategy for pure wino dark matter straightforward, including triggering and detector effects.[2] However, anywhere else on the relic neutralino surface the neutralino mass difference drops below 80 GeV so an $\chi_2^0 \to \chi_1^0$ decay via a Z boson has to occur off shell. This includes the pure higgsino sheets, as well as the bino-wino, the bino-higgsino, and the wino-higgsino mixing slopes. This small interstate splitting is one of the reasons that collider searches for electroweakino dark matter are challenging. We will address this challenge in Sec. III.

For much of the relic neutralino surface, the NLSP is the lightest chargino. Its mass difference from the dark matter

[2]In this situation, dark matter constraints alone do not give the mass of χ_2^0. The mass of χ_2^0 will set the rate for traditional trilepton search channel $pp \to \chi_1^\pm \chi_2^0$.

agent rarely exceeds 30 GeV, with the exception of lighter bino-higgsino dark matter. For the collider signatures, this means that both leptons and neutrinos from off-shell W decays will typically have small transverse momenta.

To determine the dark matter complementarity reach of a 100 TeV collider, it is useful to consider which regions of the relic neutralino surface will be accessible to current and future dark matter searches. Bounds from direct detection and neutrino telescope experiments [12–16,45–47,49] constrain TeV-mass dark matter to have a spin-independent cross section less than 10^{-44} cm^2 and a spin-dependent cross section less than 10^{-39} cm^2. After calculating the cross section for the lightest neutralino scattering off protons and neutrons in micrOMEGAs3, in Fig. 3 we show the spin-dependent and spin-independent nuclear cross sections relevant to direct detection across the relic neutralino surface. The leading order scattering cross sections given in Fig. 3 indicate that much of the relic neutralino surface is beyond the detection capability of current or planned direct detection experiments. While bino-higgsino dark matter and the bottom of the wino-higgsino valleys shown in Fig. 3 are presently already excluded by the LUX experiment [14] assuming nominal values for astrophysical and nuclear inputs, the bino-wino portion of the relic surface presents a particular challenge. As $|\mu|$ increases, the higgsino component of the LSP and the corresponding LSP coupling to the Higgs both decrease, causing a major diminution of both spin-dependent and independent nucleon cross sections. Future experiments will also have to contend with a solar neutrino background that will be relevant for spin-independent cross sections less than 10^{-48} cm^2, as detailed in the Introduction.

To begin addressing the challenge of discovering electroweakino dark matter at a future collider, in Fig. 4 we show the 100 TeV hadron collider production rates for electroweakino pair production, in the direct $2 \to 2$ production process (left panel) and in the weak boson fusion jet-associated production (right panel). The direct production rates are computed with PROSPINO2 [115] while for the Wegener-Bergeron-Findeisen (WBF) process we rely on MADGRAPH [102]. All electroweakino pair combinations are summed. The rates range from 100 pb for low masses down to 0.01 pb. Except along the bino-wino-higgsino ridge, the cross sections will be dominated by combinations of the lightest three states, $\chi^0_{1,2}$ and $\chi^\pm_1$. While the neutralino coupling to a Z boson is driven by the higgsino content, the chargino coupling to photons and to the Z boson includes the wino as well as the higgsino fraction. The mixed neutralino-chargino coupling to a W boson is diagonal in the gaugino and higgsino fractions, respectively. In the usual bino-LSP scenarios probed at the LHC the leading production processes are $\sigma(\chi^0_2\chi^\pm_1) > \sigma(\chi^+_1\chi^-_1)$. The neutralino rates $\sigma(\chi^0_2\chi^0_2) \sim \sigma(\chi^0_1\chi^0_2)$ are typically smaller [115].

If the neutralino LSP and the chargino NLSP are pure winos, as is the case on the wino LSP plateaus, direct chargino pair production and $\chi^0_1\chi^\pm_1$ production will have an unsuppressed rate. Its size is determined by the masses of the lightest neutralinos and charginos. Pure higgsino pairs couple to photons, W bosons, and Z bosons in the s channel, which in combination with the lower mass scale leads to larger cross sections on the higgsino sheets. Adding a bino fraction to the LSP will not lead directly to a significant increase of the direct production rate, because the bino fraction does not couple to W or Z bosons. However, on the relic neutralino surface the bino fraction reduces the dark matter annihilation cross section and thereby drives the required mass scales lower. This rapidly increases the 100 TeV hadron collider cross sections for direct electroweakino pair production to 0.1 pb for a LSP mass around 500 GeV.

The difference between direct production and weak boson fusion production of electroweakinos [102] is that the latter can be driven exclusively by the coupling to electroweak gauge bosons. Unfortunately, we seem to observe no improvements to speak of, compared to the direct production mode. Instead, the WBF production rates are roughly an order of magnitude below the direct production rate. In the next section we will find that the boosted kinematics are the primary factor that extends the discovery potential of a 100 TeV collider across the relic neutralino surface. We do not pursue the WBF production further in this paper; however, as electroweakinos produced via WBF tend to be boosted, these events could help to extend the 100 TeV collider discovery potential using the strategy shown in the next section.

III. ALMOST DEGENERATE DARK MATTER SEARCHES

Having mapped out the regions of electroweakino parameter space which predicts the correct relic abundance, we turn to collider studies and focus our attention on some collider-salient features of the relic density surface. First, the splitting between LSP and its electroweakino cohorts is small. From Fig. 2 we know that the neutralino-neutralino splitting is $\Delta m_{\chi^0_2-\chi^0_1} < m_Z$ for all electroweakino admixtures with the sole exception of the pure wino plateau. The chargino-neutralino splitting stays below $\Delta m_{\chi^\pm_1-\chi^0_1} < m_W$ over the entire surface. A neutralino mass splitting below the Z mass complicates hadron collider searches, because it spoils one of the most effective top-background rejection cuts in trilepton searches [116–121]. The compressed nature of the relic electroweakino sector with its soft decay leptons challenges vanilla electroweakino pair production $pp \to \chi_i\chi_j$; issues arise with triggering, as well as background rejection. In the analysis following, we explore boosted electroweakinos recoiling against hard jets as a unique opportunity at a 100 TeV collider. After accounting for the decay of any heavier electroweakinos, boosted electroweakino final states have the form $pp \to j\not{p}_T X$, where X is some combination of leptons and photons.

The hard jet in the event serves two purposes: first, it can be triggered on and, in turn, allows the cuts on photons or leptons to be relaxed. This is crucial when we want to be sensitive to decays of the heavier electroweakinos with small mass splittings. Second, it impels the electroweakinos in the opposite direction, which leads to large missing transverse momentum. We will see that the combination of large $\not{p}_T$ plus soft leptons or photons is especially powerful at a 100 TeV collider.

While the basic kinematics of boosted electroweakino signals are dictated by the hard jet in the event, the details depend on which soft particles are present. As these soft particles come from heavier electroweakino decays, their identity is dictated by which combination of chargino or neutralino states is produced. This, in turn, is dictated by the wino/bino/higgsino content of the electroweakinos. In the following subsections we present two possible scenarios,

$$pp \to \ell^{\pm}\gamma j \not{p}_T$$
$$pp \to \ell^{+}\ell^{-} j \not{p}_T, \qquad (2)$$

which will be particularly effective in finding compressed electroweakino decays at a 100 TeV hadron collider. In the combination of the two channels we will see that the 100 TeV hadron collider can resolve mass splittings below 5 GeV between TeV-mass electroweakino states.

To establish the coverage of the relic neutralino surface, we proceed in three steps: first, in Sec. III A we will apply the lepton-photon analysis to the relic neutralino surface, specifically to bino-wino dark matter. In Sec. III B we will examine this analysis strategy more generally, considering neutralino mass splittings beyond those attained across the relic surface. This has implications for dark matter outside of the MSSM, as we will determine the 100 TeV collider sensitivity to 1–25 GeV mass splitting for triplet-singlet $SU(2)$ states. In Sec. III C we will show the coverage of the relic neutralino surface at slightly larger mass splittings of 5–50 GeV using the dilepton decay mode [122–127]. Soft lepton studies of nonrelic electroweakinos at 100 TeV have been addressed previously in the literature [95]. Our study considers a wider range of interelectroweakino splittings than [95] and applies the constraint that the LSP lies on the relic neutralino surface.

A. Surfing the relic surface with a photon and lepton

The first channel we examine for discovering the MSSM dark matter spectrum is the lepton-photon signature shown in Eq. (2). The soft photon comes from radiative decays $\chi_i^0 \to \gamma\chi_1^0$. As interneutralino splittings become small, which they do across the bino-wino surface and the bottom of the wino-higgsino surface shown in Fig. 2, the radiative decay to photons becomes competitive with increasingly off-shell decays through Z bosons. In Fig. 5, we display the branching ratio of the second lightest neutralino to a photon and the lightest neutralino. It is sizable across the bino-wino surface, for a narrow piece of the wino-higgsino surface, and also across the pure higgsino plane, where there is a small splitting between neutral higgsino states. These regions will be difficult to reach with future direct detection searches, as we learned from Fig. 3.

The electroweakino combination that most easily generates a final state with a lepton and photon is $\chi_1^{\pm}\chi_2^0$. To see how prevalent this electroweakino combination is as we traverse the relic neutrino surface, we plot the $pp \to \chi_1^{\pm}\chi_2^0$ cross section at 100 TeV in the left panel of Fig. 5. The rate is large ($\gtrsim$10 fb) for most of the relic neutralino surface. In particular, the $\chi_1^{\pm}\chi_2^0$ cross section is sizable even in the bino-wino regions where the spin-independent cross sections are so small they sit below the solar neutrino background cross section (see Fig. 3).

The cross section we are really interested in is not $pp \to \chi_1^{\pm}\chi_2^0$, but electroweakinos produced in association with hard initial state radiation, $pp \to \chi_1^{\pm}\chi_2^0 + j$.

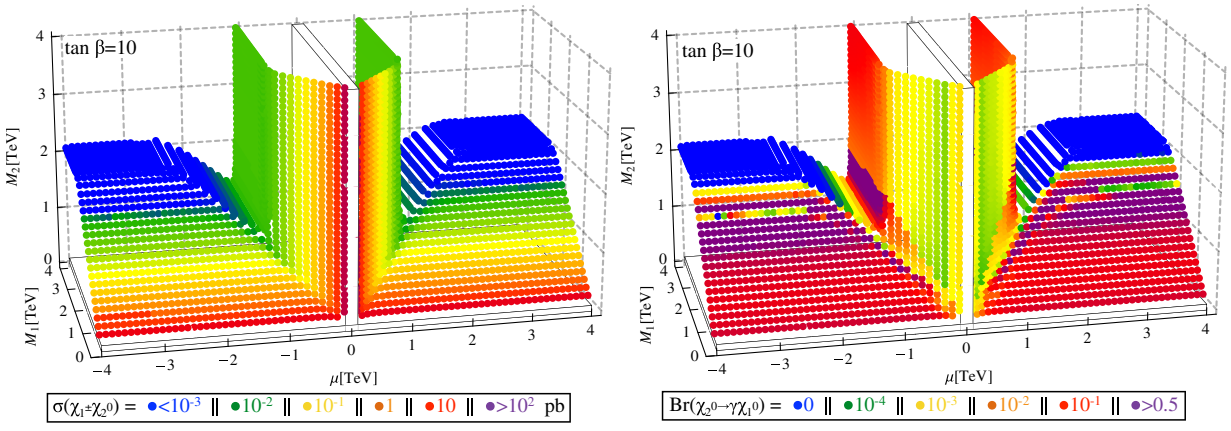

FIG. 5 (color online). Relic neutralino surface with the $\chi_2^0\chi_1^{\pm}$ production cross section (left panel) and the $\chi_2^0 \to \chi_1^0\gamma$ branching ratio (right panel).

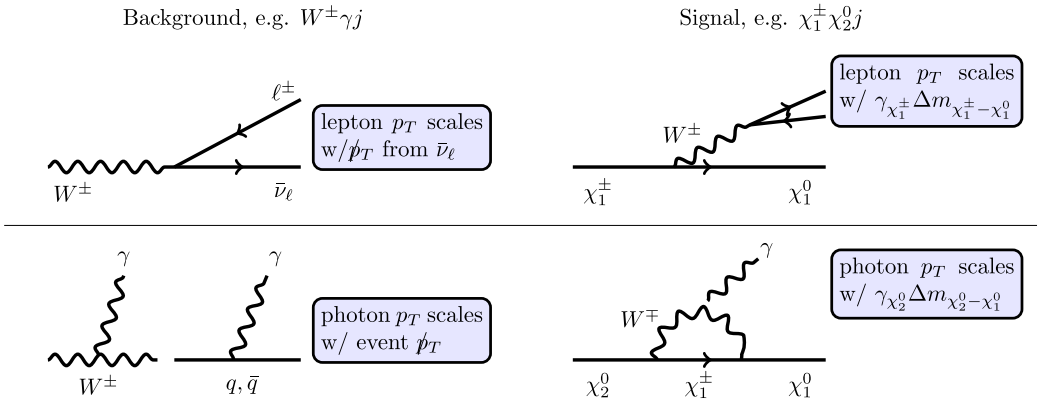

FIG. 6 (color online). Illustration of how $p_T^{\max}$ cuts on the lepton or photon reduce the $W\gamma$ background. These cuts will gain in efficacy as missing transverse momentum becomes much larger than interelectroweakino mass splittings, as will occur at a 100 TeV collider, because the electroweakino Lorentz boosts ($\gamma_{\chi_2^0}$ and $\gamma_{\chi_1^{\pm}}$) and mass splittings typically produce smaller lepton and photon transverse momenta.

Accounting for the extra radiation, the cross sections shown in Fig. 5 need to be adjusted, however this adjustment is a function of the p_T of the radiated jet and will be the same for all electroweakino processes. The final state

$$pp \to \chi_2^0\chi_1^{\pm} j \to (\gamma\chi_1^0)(\ell^{\pm}\nu\chi_1^0)j \tag{3}$$

is effective because the background can be reduced by requiring a soft photon and a lepton in association with a large amount of missing transverse momentum and a hard jet. The underlying decay processes are illustrated in Fig. 6. The dominant background to the neutralino-chargino signature is $pp \to W_\ell^{\pm}\gamma j$. A missing transverse momentum cut in the TeV range makes direct use of the increased collider energy of 100 TeV. For the background, the W boson has to be strongly boosted itself, giving $p_{T,\ell} \sim p_{T,\nu} \sim \not{p}_T$. The background photon will sometimes inherit a significant amount of transverse momentum from recoiling against a very hard jet and a very hard W boson. In contrast, electroweakino decays produce large missing transverse momentum through the boosted pair production process with two unbalanced LSPs. The lepton momentum will be set by the interelectroweakino mass splitting, $p_{T,\ell} \propto \gamma_\chi \Delta m_{\chi-\chi_1^0}/2$, where γ_χ is the boost factor of the heavy decaying electroweakino, as illustrated in Fig. 6. Altogether, this allows for efficacious electroweakino searches at a 100 TeV hadron collider sensitive to $p_T = 5$–50 GeV photons and leptons in events triggered by large $\not{p}_T$.

To determine how well the hard missing transverse momentum cut together with lepton and photon cuts discriminate the electroweakino signal from the $W\gamma j$ background, we generate tree-level signal and background events in MADGRAPH5 [128][3] combined with PYTHIA6.4 [129] and the anti-k_T jet algorithm [130,131] for clustering partons into jets, with $R = 0.5$. We simulate the detector acceptance using DELPHES3 [132], with the Snowmass detector card [133]. For generator-level cuts we require one jet with $p_{T,j} > 600$ GeV and a minimum missing transverse momentum $\not{p}_T > 1.5$ TeV. Our results only rely on the leading order $pp \to \chi_2^0\chi_1^{\pm} j$ cross sections, which will be increased by next-to-leading order (NLO) contributions [115,134,135], threshold and transverse momentum resummation [136,137], and weak boson fusion [102].

To illustrate why this analysis works with maximum cuts on lepton and photon momenta, we show the lepton and photon transverse momentum distributions for a $m_\chi = 200$ GeV bino-wino with a 10 GeV interneutralino mass splitting in Fig. 7. For the LHC with 14 TeV we find many $W\gamma j$ background events with a soft lepton and a soft photon. As the collider energy and the cuts on the hard jet and the missing transverse momentum increase, the background lepton and photon become harder. Both of them show a correlation with the missing transverse momentum cut of $\not{p}_T > 1.5$ TeV, making it easier to remove this background with a maximum photon and lepton p_T requirement.

We now proceed to the analysis of the bino-wino portion of the relic neutralino surface. To probe this parameter regime we decouple the higgsino fraction at $|\mu| = 4$ TeV. Adjusting M_1 and M_2 allows us to follow the line with the correct relic density. As the mass splitting varies as we traverse the surface, one would ideally optimize the cuts at each M_1, M_2 point to maximize the efficiency. Here, for simplicity, we work with only two sets of cuts—one set for M_1 below ~900 GeV, where the LSP is more binolike, and one set for $M_1 > 900$ GeV, where the LSP is more wino:

[3]We used the default MADGRAPH5 parton density functions, factorization, and renormalization schemes for all simulated events.

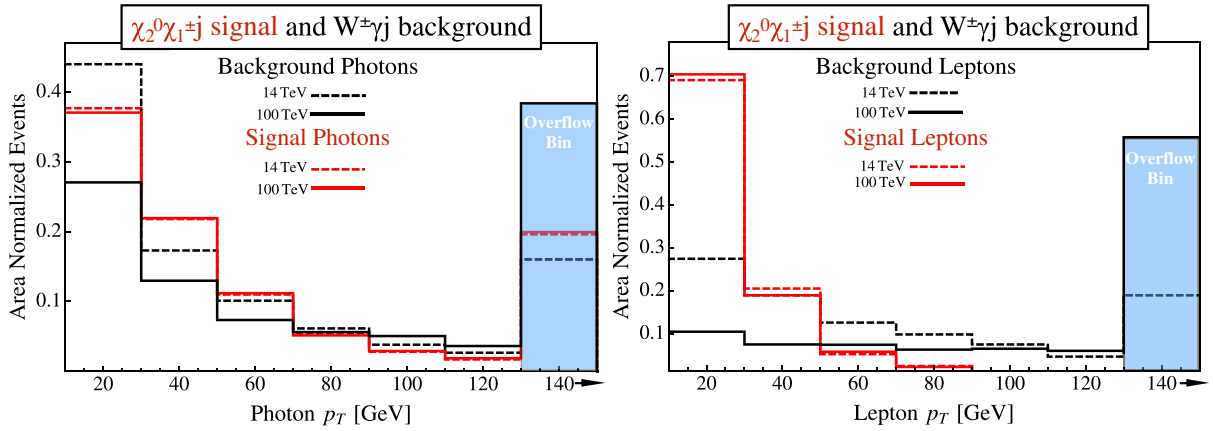

FIG. 7 (color online). Photon and lepton transverse momenta for the $\chi_2^0\chi_1^\pm j$ signal and the $W\gamma j$ background at 14 TeV and 100 TeV. We assume a bino-wino mass spectrum $m_{\chi_2^0} = m_{\chi_1^\pm} = 200$ GeV with a mass splitting $\Delta m_{\chi_2^0-\chi_1^0} = 10$ GeV. At this level we require at least one jet with $p_{T,j} > 100$ GeV for the 14 TeV collider and $p_{T,j} > 600$ GeV for 100 TeV. Note that the tails of these distributions, here shown collected in an overflow bin, fall off out to $p_T \sim$ TeV.

$$
\begin{aligned}
p_{T,\ell} &= \begin{cases} [5,80]\ \text{GeV} & (M_1 < 900\ \text{GeV}) \\ [5,40]\ \text{GeV} & (M_1 \geq 900\ \text{GeV}) \end{cases} & |\eta_\ell| &< 2.5 \\
p_{T,\gamma} &= \begin{cases} [5,80]\ \text{GeV} & (M_1 < 900\ \text{GeV}) \\ [5,60]\ \text{GeV} & (M_1 \geq 900\ \text{GeV}) \end{cases} & |\eta_\gamma| &< 2.5 \qquad \Delta R_{\ell-\gamma} > 0.5 \\
p_{T,j} &> 1\ \text{TeV} & |\eta_j| &< 4.5 \\
\not{p}_T &> 1.5\ \text{TeV}
\end{aligned}
\tag{4}
$$

To reject hadronic backgrounds, the cuts require no more than two jets with $p_T > 300$ GeV. The jet cut given in Eq. (4) is really only relevant for triggering; lowering it to $p_{T,j} > 300$ GeV does not affect the collider reach. An improved lepton-photon analysis would vary the jet and missing transverse momentum cuts as a function of the electroweakino masses.

The lower cut on the soft lepton and photon p_T is an optimistic assumption on the detector performance, however the utility of the low threshold motivates taking these values seriously. The Snowmass DELPHES3 card [133] assumes zero efficiency for leptons with less than 10 GeV of energy. Therefore, for the purposes of this study we modify the card, matching the sensitivity for 5–10 GeV photons and leptons to the value at 10 GeV. However, even without sensitivity to photons and leptons < 10 GeV, the required luminosity for detecting all points shown remains less than ten inverse attobarns.

Like any photon-based analysis this electroweakino search relies on an efficient rejection of fake photons from jets. Focusing on the $M_1 \geq 900$ GeV analysis, we generate hard $W +$ jets events, again with MADGRAPH5, PYTHIA6.4, and DELPHES3. Lowering the DELPHES3 jet threshold to 5 GeV and treating every radiated jet with $p_{T,j} < 60$ GeV as a possible fake photon we determine the required fake photon rejection rate. We find a rejection rate around $1/125$ for $p_{T,\gamma} > 5$ GeV is needed to safely suppress the fake background. This estimate is only approximate as it ignores any kinematic dependence in the fake rate and assumes our tool settings (in MADGRAPH5 and PYTHIA6.4) accurately describe the 100 TeV collision environment. However, the fake rate we need to suppress $W +$ jets events is orders of magnitude more conservative than what is currently achievable at the LHC [138].

In Fig. 8 we show the luminosity required to discover bino-winos on the relic neutralino surface at a 100 TeV hadron collider. Here we take the simplest definition of significance as $S/\sqrt{B}$, and note that all points in Fig. 8 have $S/B > 1/5$ and more than 50 signal events expected. With around seven inverse attobarns of integrated luminosity, the relic bino-wino surface will be detected with 5σ significance for LSP masses up to 1.5 TeV. We checked that assuming 10% systematic errors for the signal and 2% for the background still permits 5σ significance detection with 10 ab^{-1} luminosity. Above a LSP mass of 1.5 TeV, parameter space transitions to the pure wino surface, as indicated by the rapidly increasing NLSP-LSP mass splitting. Although we have carried out this analysis for $\mu = 4$ TeV we expect the results to apply over much of the bino-wino surface, as indicated by the shaded region in Fig. 8, as the relevant properties do not vary much as μ is lowered.

The reach of our photon signature can be compared to the parameter coverage through charged tracks [95]. While charged track searches should be able to detect the wino

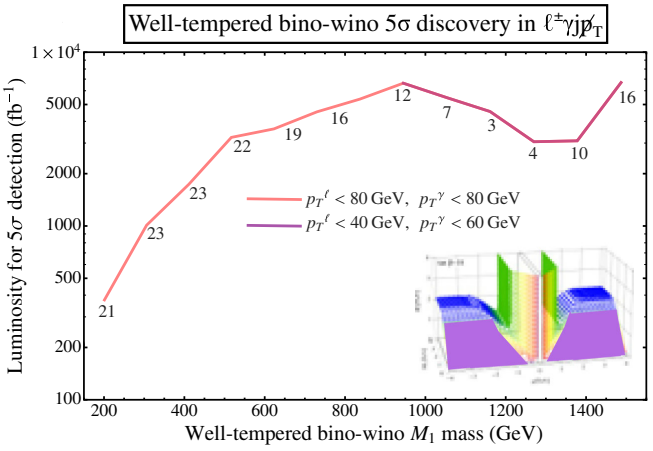

FIG. 8 (color online). Well-tempered bino-wino mass reach at a 100 TeV proton collider in the $\ell\gamma jp\!\!\!/_T$ final state for $M_1 = 0.2$–1.5 TeV. The mass splitting in GeV between the χ_2^0 and the LSP is indicated at each point on the curve. Note that the mass splitting between $\chi_1^{\pm}$ and the LSP will be ~0.5 GeV larger than that of χ_2^0, because χ_2^0 is mostly wino.

component over portions of the bino-wino relic surface at a 100 TeV collider, underlying assumptions about the superpartner mass spectrum are crucial. Custodial symmetry breaking in the Standard Model induces a 160 MeV splitting between the neutral and charged wino states [139]. However, such a small chargino-LSP splitting is not guaranteed; it assumes that both $|\mu|$ and every other $SU(2)_L$ MSSM mass is decoupled above 10 TeV. For example a higgsino mass of $|\mu| \sim 1.5$ TeV will result in an additional 200 MeV tree-level splitting between the charged and neutral wino states of an 800 GeV bino-wino. The electroweak NLO corrections to the second-lightest neutralino in the presence of light scalars easily exceed 1 GeV, while keeping the LSP mass constant [105–107]. Decoupling the scalars will reduce the typical size of these electroweak corrections, but the corrections from the electroweakino sector itself will not necessarily drop below 1 GeV. This is why a second channel covering electroweakino dark matter with small mass differences significantly adds to the case for a 100 TeV collider.

B. Probing small neutralino mass splittings

Going beyond the discovery of relic bino-winos, we now apply the same photon plus lepton search to a broader range of bino-wino mass splittings and masses, but without imposing the constraint of viable relic abundance. To determine how small a mass difference between weakly charged particles a 100 TeV collider can resolve, we assume similar cuts and procedures as the preceding section. Throughout this section as throughout the last, we decouple the higgsino content at $\mu = 4$ TeV.

We compute the luminosity that will be required for a detection of compressed bino-winos as a function of the LSP mass and the mass splitting to the second lightest neutral state (the splitting between the LSP and the lightest chargino is similar). These target luminosities again assume $W\gamma j$ as the dominant background. We cover mass splittings of 1–25 GeV in two steps. First, for neutralino mass splittings 2 GeV or greater, we require exactly one lepton (e or μ), one photon, and at least one jet, with

$$\begin{aligned} &p_{T,\ell} = [10, 40]\ \text{GeV} \quad |\eta_\ell| < 2.5 \\ &p_{T,\gamma} = [10, 60]\ \text{GeV} \quad |\eta_\gamma| < 2.5 \quad \Delta R_{\ell-\gamma} > 0.5 \\ &p_{T,j} > 1\ \text{TeV} \quad |\eta_j| < 4.5 \\ &\not{p}_T > \begin{cases} 1.5\ \text{TeV} & (m_{\chi_2^0} = 200\ \text{GeV}) \\ 2.0\ \text{TeV} & (m_{\chi_2^0} > 200\ \text{GeV}). \end{cases} \end{aligned} \tag{5}$$

For mass splittings between 1 GeV and 2 GeV and a low LSP mass of $m_{\chi_1^0} = 200$ GeV, the lepton and photon acceptance cuts in Eq. (5) are not efficient enough. For such small splittings, we lower the lepton and photon cuts to $p_{T,\ell} = [3, 10]$ GeV and $p_{T,\gamma} = [5, 10]$ GeV; we consider these acceptance cuts a benchmark value and expect they could be optimized further. From the right panel of Fig. 2 we see that such a small leading order mass splitting indeed occurs in the pure wino and higgsino regions. As discussed above, it remains to be seen how large quantum corrections to these mass splittings can be [105–107].

In Fig. 9 we show the luminosity which is required for a 5σ discovery of associated neutralino-chargino production with the photon decay signature shown in Eq. (3). Again, we define significance simply as $S/\sqrt{B}$ and note that $S/B > 1/4$ for all points shown, except for $m_{\chi_1^0} \sim 2$ TeV where $S/B > 1/20$. The two relevant parameters are the mass difference between the lightest two neutralinos, determining the kinematics, and the mass scale of the two produced particles, determining the production cross section. For this first result we do not require the neutralino LSP to reproduce the observed dark matter relic density. We show the conservative detector acceptance cuts from Eq. (5), assuming sensitivity to $p_T > 10$ GeV photons and leptons, as well as results for an improved lower cut for the lepton and photon momenta of $p_T > 5$ GeV.

In this general analysis we see that the properties that make a 100 TeV collider ideal for dark matter mass spectroscopy are simple but powerful: the signature including a very hard jet and sizable missing transverse momentum as well as a lepton and a photon will feature extremely boosted electroweak backgrounds. In contrast, heavy electroweakino pairs will be produced closer to threshold, and the decays of lighter neutralinos and charginos will be so boosted that the neutralino mass splittings in the detector's rest frame will be resolvable as otherwise undetectably soft leptons and photons. While bino-winos of up to 150 GeV in mass and with > 10 GeV interstate splittings can be probed at the LHC [140,141], a 100 TeV collider can resolve mass

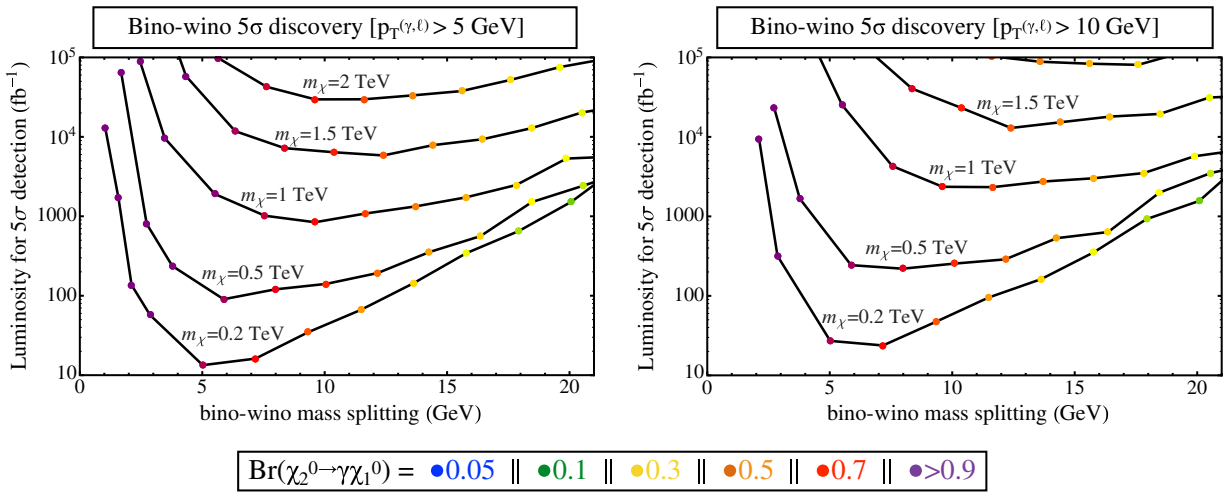

FIG. 9 (color online). 100 TeV hadron collider mass reach for a range of bino-wino mass splittings. The LSP mass is indicated on each curve. The cuts applied are shown in Eq. (5) and the corresponding text. The branching fraction for the decay $\chi_2^0 \to \chi_1^0\gamma$ is indicated at each significance point.

splittings as small as a GeV and is sensitive to much heavier neutralinos.

C. Cruising the relic surface with soft leptons

Moving from few-GeV mass splittings to mass splittings between 5 and 50 GeV we now establish the impact of the second, dilepton signature in Eq. (2). Our analysis largely follows its LHC counterpart [125] and aims for the gap between lepton-photon or monojet analyses for very small mass differences, and the trilepton search which is most successful for mass splittings above 50 GeV. On the relic neutralino surface, the lepton-photon channel described in Sec. III A and the soft lepton signature will complement each other on the bino-wino slope. In addition, soft dileptons will be the leading search strategy on the bino-higgsino sheet. Some relevant signal processes contributing to the soft dilepton signature, ordered by typical size, are

$$\begin{aligned}
pp &\to \chi_1^+\chi_1^- j \to (\ell^+\nu\chi_1^0)(\ell^-\bar{\nu}\chi_1^0)j \\
pp &\to \chi_2^0\chi_1^\pm j \to (\ell^\pm\nu jj\chi_1^0)(\ell^\pm\nu\chi_1^0)j \\
pp &\to \chi_2^0\chi_1^\pm j \to (\ell^+\ell^-\nu\bar{\nu}\chi_1^0)(jj\chi_1^0)j \\
pp &\to \chi_2^0\chi_1^\pm j \to (\ell^+\ell^-\chi_1^0)(jj\chi_1^0)j \\
pp &\to \chi_2^0\chi_1^\pm j \to (\ell^+\ell^-\chi_1^0)(\ell^\pm\nu\chi_1^0)j \\
pp &\to \chi_2^0\chi_1^\pm j \to (\ell^+\ell^-\nu\bar{\nu}\chi_1^0)(\ell^\pm\nu\chi_1^0)j \\
pp &\to \chi_2^0\chi_1^0 j \to (\ell^+\ell^-\chi_1^0)\chi_1^0 j. \qquad (6)
\end{aligned}$$

Channels involving a χ_2^0 pair are not considered since the underlying production cross section is negligible. When the spectrum is compressed, as we have shown it is for almost the entirety of the relic neutralino surface, these decay leptons will be soft. For our analysis we include all production and decay combinations based on the direct production $pp \to \chi_i\chi_j$. The backgrounds for the dilepton final state are diboson production dominated by $pp \to W^+W^- j$ production, $\tau^+\tau^- j$ production, and $t\bar{t}$ production. For our analysis we consider these three channels as the combined background.

Similar to the analysis in Sec. III A we generate tree-level signal and background events with MADGRAPH5 [128], PYTHIA8 [142], and DELPHES3 [132] with the Snowmass detector card [133]. Jets are defined using the anti-k_T jet algorithm [130,131] with $R = 0.4$. Since we will ask for exactly one hard jet and veto events with additional hard jets, we restrict the simulations to one hard jet in the matrix element. As generator-level cuts we ask for $p_{T,j} > 80$ GeV, $p_{T,\ell} > 5$ GeV, and for the backgrounds $\not{p}_T > 480$ GeV. For the $t\bar{t}$ background we apply an anti-b-tag on the hardest jet, conservatively implemented through a 20% efficiency of passing the anti-b-tag multiplied onto the $t\bar{t}$ cross section. Outside the strongly boosted regime this detector acceptance for leptons limits us to mass splittings above 5 GeV.

To reject the wide variety of different background processes we require exactly one anti-b-tagged jet, sizable missing transverse momentum, and at least two isolated leptons (e or μ) with

$$\begin{aligned}
&p_{T,\ell} = [10, 50]\ \text{GeV} \qquad |\eta_\ell| < 2.5 \qquad m_{\ell\ell} < m_{\ell\ell}^{\max} \\
&p_{T,j} > 100\ \text{GeV} \qquad |\eta_j| < 2.5 \qquad \not{p}_T > 500\ \text{GeV}. \qquad (7)
\end{aligned}$$

Events including additional jets with $p_{T,j} > 100$ GeV, mostly coming from $t\bar{t}$ production, are vetoed. The two highest-p_T leptons are selected from events with more than two leptons. The reasoning behind the stiff cut on missing transverse momentum again follows Fig. 6. We could increase it to $\not{p}_T > 1$ TeV, which increases the

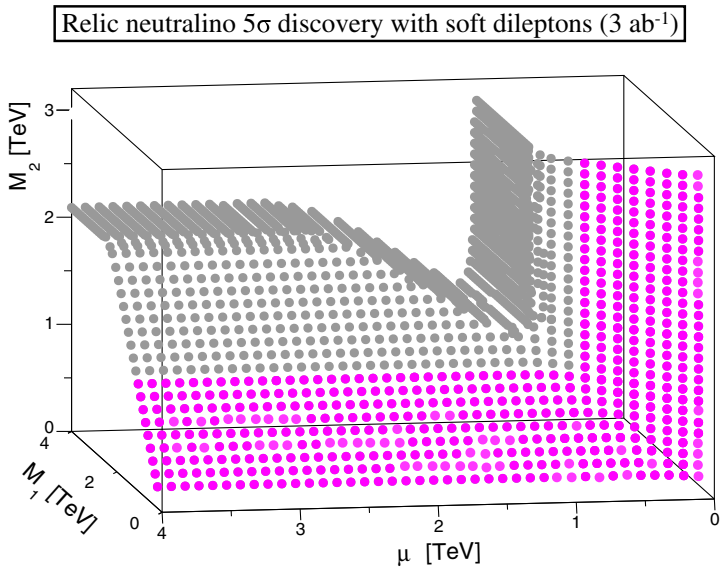

FIG. 10 (color online). Discovery range of the dilepton signal, defined by $S/\sqrt{B} > 5$ at 3 ab^{-1}. The colored points can be discovered with no more than 3 ab^{-1} of data, while the grey points will require more luminosity.

signal-to-background ratio S/B but reduces $S/\sqrt{B}$. In terms of the reach of a 100 TeV collider the two scenarios are roughly equal. Finally, we could ask for a harder jet without a large effect on the signal rate, but unlike in Sec. III A the two leptons in this signature, combined with very large missing momentum, should guarantee an efficient trigger.

For all processes listed in Eq. (6) we know that the χ_2^0 and $\chi_1^\pm$ decays involve off-shell bosons with soft leptons. In contrast the background leptons tend to come from on-shell gauge boson decays. In addition to the individual upper limit on $p_{T,\ell}$ we can further reduce the WW/ZZ and $t\bar{t}$ backgrounds using an upper limit on $m_{\ell\ell}$ for the two hardest leptons [125]. Because of the number of distinct signal paths (6) and the variety of mass splittings over the relic surface, the optimal cut for $m_{\ell\ell}$ varies, often over values such that $m_{\ell\ell} < 90$ GeV. This is why after all other cuts, we apply the optimal value for an $m_{\ell\ell}$ cut determined individually for each parameter point and chosen to maximize the statistical significance $S/\sqrt{B}$. In cases where the $m_{\ell\ell}$ cut does not improve significance, for example due to too small signal rates, this procedure will automatically remove the cut altogether.

The two limiting factors for this analysis are the signal production cross section shown in Fig. 4 and the mass splitting shown in Fig. 2. In Fig. 10 we show the 5σ discovery range with an integrated luminosity of 3 ab^{-1}. For the points in reach of a 100 TeV collider we find typical signal-to-background ratios $S/B \gtrsim 1/5$. As mentioned above, the balance between statistical and systematic uncertainties can be balanced by the choice of $\not{p}_T$ cut. The significance and the signal-to-background ratio worsen on the bino-wino surface towards higher M_1 and on the bino-higgsino surface towards higher μ, in both cases corresponding to a decreased mass splitting.

IV. CONCLUSIONS

In this article we have mapped the surface of bino-wino-higgsino parameter space which provides the correct relic abundance, assuming all other superpartners are decoupled. The majority of this relic neutralino surface is compressed: the mass splitting between the NLSP and the LSP is typically much less than the mass of electroweak bosons. Furthermore, large portions of the relic MSSM neutralino surface, in particular, the bino-wino portion, will be inaccessible to all planned direct detection searches. This makes the surface a ripe target at future colliders for dark matter searches that require large missing transverse momentum and associated electroweak particles with low momenta.

To discover relic neutralinos at a next-generation 100 TeV collider, we have demonstrated two effective methods: searches for large missing transverse momentum, a jet from initial state radiation, and either a soft photon and lepton or two soft leptons. These final states are produced in the decays of slightly heavier electroweakinos down to the LSP. Our searches especially benefit from the increased center of mass energy at a 100 TeV collider as we can look for boosted electroweakinos. Once boosted, the electroweakino signal induces large missing energy, but relatively soft leptons, as their energy is set by the interelectroweakino mass splittings. This combination of large missing energy and soft leptons is difficult to achieve in the SM where both the $\not{p}_T$ and leptons come from the same object, typically an electroweak gauge boson.

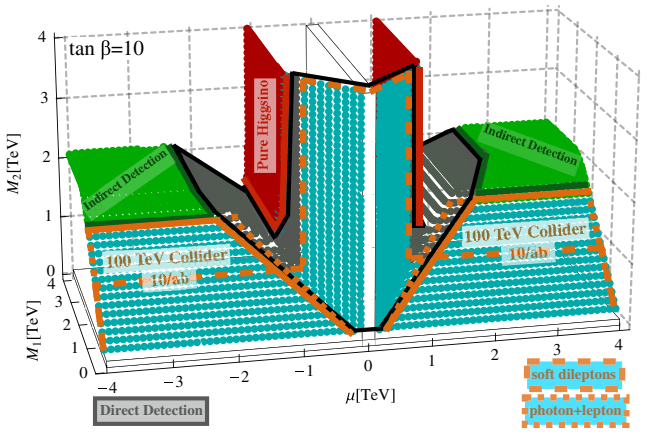

FIG. 11 (color online). Relic neutralino surface divided into prospective regions of future direct, future indirect, and collider detection accessibility as indicated. Direct detection regions were determined by requiring the spin-independent cross section be $> 10^{-45}$ cm^2, as calculated at tree level by micrOMEGAs3. Regions detectable by a 100 TeV collider using missing transverse momentum, a hard jet, and either soft dileptons or a lepton and photon are marked with long- and short-dashed lines, respectively. The white box occludes regions already ruled out by LEP.

Quantitatively, we have shown that the photon and lepton search will discover up to 1.5 TeV relic bino-wino dark matter with less than ten inverse attobarns of luminosity. Assuming a next-generation detector sensitive to photons with momenta as small as 5 GeV, we find that neutralino mass splittings as small as 1 GeV can be discovered in the boosted environment present at a 100 TeV collider. We also showed that a 100 TeV collider is particularly adept at finding relic bino-winos and bino-higgsinos using the soft dileptons emitted in heavier neutralino and charging decays, for relic masses up to ~TeV. While this leaves some bino-higgsino and wino-higgsino portions of the surface undiscoverable at a 100 TeV collider, this same relic neutralino parameter space is the most accessible to next generation direct detection experiments, as illustrated in Fig. 11. We conclude that a 100 TeV collider will be a spectacular complement to other dark matter searches and often provides the best prospects for dark matter discovery, both over the MSSM relic neutralino surface and for electroweak dark matter states with 1–50 GeV mass splittings.

ACKNOWLEDGMENTS

We would like to thank Vera Gluscevic, Rafael Lang, Annika Peter, and Pedro Schwaller for the discussions. J. B. is grateful to the CERN theory group for their hospitality while this paper was finalized. T. P. would like to thank the Fermilab Theory Group, where this project once started. T. S. acknowledges support from the IMPRS for Precision Tests of Fundamental Symmetries. The work of A. M. was partially supported by the National Science Foundation under Grant No. PHY-1417118. This research was supported in part by the Notre Dame Center for Research Computing with computing resources. This work was partially supported by World Premier International Research Center Initiative (WPI), MEXT, Japan. Fermilab is operated by Fermi Research Alliance, LLC under Contract No. DE-AC02-07CH11359 with the U.S. Department of Energy.

[1] D. E. Morrissey, T. Plehn, and T. M. Tait, Physics searches at the LHC, Phys. Rep. **515**, 1 (2012).
[2] LEP2 SUSY Working Group Collaboration, LEPSUSYWG, ALEPH, DELPHI, L3, and OPAL experiments, http://lepsusy.web.cern.ch/lepsusy/.
[3] T. Cohen, M. Lisanti, A. Pierce, and T. R. Slatyer, Wino dark matter under siege, J. Cosmol. Astropart. Phys. 10 (2013) 061.
[4] J. Fan and M. Reece, In wino veritas? Indirect searches shed light on neutralino dark matter, J. High Energy Phys. 10 (2013) 124.
[5] G. Aad *et al.* (ATLAS Collaboration), Search for charginos nearly mass degenerate with the lightest neutralino based on a disappearing-track signature in pp collisions at $\sqrt{(s)} = 8$ TeV with the ATLAS detector, Phys. Rev. D **88**, 112006 (2013).
[6] N. Arkani-Hamed, A. Delgado, and G. Giudice, The well-tempered neutralino, Nucl. Phys. **B741**, 108 (2006).
[7] K. Griest and M. Kamionkowski, Unitarity Limits on the Mass and Radius of Dark Matter Particles, Phys. Rev. Lett. **64**, 615 (1990).
[8] H.-Y. Chiu, Symmetry between Particle and Antiparticle Populations in the Universe, Phys. Rev. Lett. **17**, 712 (1966).
[9] G. Steigman, Cosmology confronts particle physics, Annu. Rev. Nucl. Part. Sci. **29**, 313 (1979).
[10] R. J. Scherrer and M. S. Turner, On the relic, cosmic abundance of stable weakly interacting massive particles, Phys. Rev. D **33**, 1585 (1986).
[11] J. L. Feng and J. Kumar, The WIMPless Miracle: Dark-Matter Particles without Weak-Scale Masses or Weak Interactions, Phys. Rev. Lett. **101**, 231301 (2008).
[12] M. Xiao *et al.* (PandaX Collaboration), First dark matter search results from the PandaX-I experiment, Sci. China Phys. Mech. Astron. **57**, 2024 (2014).

[13] R. Agnese *et al.* (SuperCDMS Collaboration), Search for Low-Mass WIMPs with SuperCDMS, Phys. Rev. Lett. **112**, 241302 (2014).

[14] D. Akerib *et al.* (LUX Collaboration), First Results from the LUX Dark Matter Experiment at the Sanford Underground Research Facility, Phys. Rev. Lett. **112**, 091303 (2014).

[15] E. Aprile *et al.* (XENON100 Collaboration), Dark Matter Results from 225 Live Days of XENON100 Data, Phys. Rev. Lett. **109**, 181301 (2012).

[16] E. Aprile *et al.* (XENON100 Collaboration), Limits on Spin-Dependent WIMP-Nucleon Cross Sections from 225 Live Days of XENON100 Data, Phys. Rev. Lett. **111**, 021301 (2013).

[17] L. J. Hall, K. Jedamzik, J. March-Russell, and S. M. West, Freeze-in production of FIMP dark matter, J. High Energy Phys. 03 (2010) 080.

[18] K. M. Zurek, Asymmetric dark matter: Theories, signatures, and constraints, Phys. Rep. **537**, 91 (2014).

[19] K. Petraki and R. R. Volkas, Review of asymmetric dark matter, Int. J. Mod. Phys. A **28**, 1330028 (2013).

[20] P. J. Fox and E. Poppitz, Leptophilic dark matter, Phys. Rev. D **79**, 083528 (2009).

[21] K. Griest and D. Seckel, Three exceptions in the calculation of relic abundances, Phys. Rev. D **43**, 3191 (1991).

[22] S. Henrot-Versille, R. Lafaye, T. Plehn, M. Rauch, D. Zerwas, S. Plaszczynski, Benjamin Rouillé d'Orfeuil, and M. Spinelli, Constraining supersymmetry using the relic density and the Higgs boson, Phys. Rev. D **89**, 055017 (2014).

[23] P. Bechtle, T. Bringmann, K. Desch, H. Dreiner, M. Hamer *et al.*, Constrained supersymmetry after two years of LHC data: A global view with Fittino, J. High Energy Phys. 06 (2012) 098.

[24] T. Cohen and J. G. Wacker, Here be dragons: The unexplored continents of the CMSSM, J. High Energy Phys. 09 (2013) 061.

[25] A. Fowlie, M. Kazana, K. Kowalska, S. Munir, L. Roszkowski, E. M. Sessolo, S. Trojanowski, and Y.-L. S. Tsai, The CMSSM favoring new territories: The impact of new LHC limits and a 125 GeV Higgs, Phys. Rev. D **86**, 075010 (2012).

[26] C. Strege, G. Bertone, F. Feroz, M. Fornasa, R. Ruiz de Austri, and R. Trotta, Global fits of the cMSSM and NUHM including the LHC Higgs discovery and new XENON100 constraints, J. Cosmol. Astropart. Phys. 04 (2013) 013.

[27] B. Bhattacherjee, M. Chakraborti, A. Chakraborty, U. Chattopadhyay, D. Das, and D. Kumar Ghosh, Implications of the 98 GeV and 125 GeV Higgs scenarios in nondecoupling supersymmetry with updated ATLAS, CMS, and PLANCK data, Phys. Rev. D **88**, 035011 (2013).

[28] O. Buchmueller, R. Cavanaugh, A. De Roeck, M. Dolan, J. Ellis *et al.*, The CMSSM and NUHM1 after LHC Run 1, Eur. Phys. J. C **74**, 2922 (2014).

[29] L. Roszkowski, E. M. Sessolo, and A. J. Williams, What next for the CMSSM and the NUHM: Improved prospects for superpartner and dark matter detection, J. High Energy Phys. 08 (2014) 067.

[30] C. Boehm, P. S. B. Dev, A. Mazumdar, and E. Pukartas, Naturalness of light neutralino dark matter in pMSSM after LHC, XENON100 and Planck data, J. High Energy Phys. 06 (2013) 113.

[31] A. Fowlie, K. Kowalska, L. Roszkowski, E. M. Sessolo, and Y.-L. S. Tsai (BayesFITS Group Collaboration), Dark matter and collider signatures of the MSSM, Phys. Rev. D **88**, 055012 (2013).

[32] M. Cahill-Rowley, J. Hewett, A. Ismail, and T. Rizzo, Constraints on Higgs properties and SUSY partners in the pMSSM, arXiv:1308.0297.

[33] M. Cahill-Rowley, R. Cotta, A. Drlica-Wagner, S. Funk, J. Hewett *et al.*, Complementarity of dark matter searches in the pMSSM, arXiv:1405.6716.

[34] M. Chakraborti, U. Chattopadhyay, A. Choudhury, A. Datta, and S. Poddar, The electroweak sector of the pMSSM in the light of LHC—8 TeV and other data, J. High Energy Phys. 07 (2014) 019.

[35] L. Roszkowski, E. M. Sessolo, and A. J. Williams, Prospects for dark matter searches in the pMSSM, J. High Energy Phys. 08 (2014) 067.

[36] L. Roszkowski, Light neutralino as dark matter, Phys. Lett. B **262**, 59 (1991).

[37] S. Mizuta and M. Yamaguchi, Coannihilation effects and relic abundance of Higgsino dominant LSP(s), Phys. Lett. B **298**, 120 (1993).

[38] J. Edsjo and P. Gondolo, Neutralino relic density including coannihilations, Phys. Rev. D **56**, 1879 (1997).

[39] J. R. Ellis, T. Falk, and K. A. Olive, Neutralino-stau coannihilation and the cosmological upper limit on the mass of the lightest supersymmetric particle, Phys. Lett. B **444**, 367 (1998).

[40] J. R. Ellis, T. Falk, K. A. Olive, and M. Srednicki, Calculations of neutralino-stau coannihilation channels and the cosmologically relevant region of MSSM parameter space, Astropart. Phys. **13**, 181 (2000).

[41] J. L. Feng, K. T. Matchev, and F. Wilczek, Neutralino dark matter in focus point supersymmetry, Phys. Lett. B **482**, 388 (2000).

[42] J. R. Ellis, K. A. Olive, and Y. Santoso, Calculations of neutralino stop coannihilation in the CMSSM, Astropart. Phys. **18**, 395 (2003).

[43] A. Birkedal-Hansen and B. D. Nelson, Relic neutralino densities and detection rates with nonuniversal gaugino masses, Phys. Rev. D **67**, 095006 (2003).

[44] T. Nihei, L. Roszkowski, and R. Ruiz de Austri, Exact cross-sections for the neutralino slepton coannihilation, J. High Energy Phys. 07 (2002) 024.

[45] E. Behnke, J. Behnke, S. Brice, D. Broemmelsiek, J. Collar *et al.*, Improved Limits on Spin-Dependent WIMP-Proton Interactions from a Two Liter CF_3I Bubble Chamber, Phys. Rev. Lett. **106**, 021303 (2011).

[46] M. Felizardo, T. Girard, T. Morlat, A. Fernandes, A. Ramos *et al.*, Final Analysis and Results of the Phase II SIMPLE Dark Matter Search, Phys. Rev. Lett. **108**, 201302 (2012).

[47] S. Archambault *et al.* (PICASSO Collaboration), Constraints on low-mass WIMP interactions on ^{19}F from PICASSO, Phys. Lett. B **711**, 153 (2012).

[48] T. Tanaka *et al.* (Super-Kamiokande Collaboration), An indirect search for WIMPs in the Sun using 3109.6 days of upward-going muons in super-Kamiokande, Astrophys. J. **742**, 78 (2011).
[49] M. Aartsen *et al.* (IceCube Collaboration), Search for Dark Matter Annihilations in the Sun with the 79-String IceCube Detector, Phys. Rev. Lett. **110**, 131302 (2013).
[50] J. Hisano, K. Ishiwata, N. Nagata, and T. Takesako, Direct detection of electroweak-interacting dark matter, J. High Energy Phys. 07 (2011) 005.
[51] J. Hisano, K. Ishiwata, and N. Nagata, Direct search of dark matter in high-scale supersymmetry, Phys. Rev. D **87**, 035020 (2013).
[52] R. J. Hill and M. P. Solon, WIMP-Nucleon Scattering with Heavy WIMP Effective Theory, Phys. Rev. Lett. **112**, 211602 (2014).
[53] R. J. Hill and M. P. Solon, Standard Model anatomy of WIMP dark matter direct detection I: Weak-scale matching, Phys. Rev. D **91**, 043504 (2015).
[54] R. J. Hill and M. P. Solon, Standard Model anatomy of WIMP dark matter direct detection II: QCD analysis and hadronic matrix elements, Phys. Rev. D **91**, 043505 (2015).
[55] P. Cushman, C. Galbiati, D. McKinsey, H. Robertson, T. Tait *et al.*, Working Group report: WIMP dark matter direct detection, arXiv:1310.8327.
[56] F. Mayet, J. Billard, and D. Santos, Directional detection of dark matter, EAS Publ. Ser. **53**, 3 (2012).
[57] D. S. Alves, S. E. Hedri, and J. G. Wacker, Dark matter in 3D, arXiv:1204.5487.
[58] F. Mayet and J. Billard, A review on the discovery reach of Dark Matter directional detection, J. Phys. Conf. Ser. **469**, 012013 (2013).
[59] P. J. Fox, J. Liu, and N. Weiner, Integrating out astrophysical uncertainties, Phys. Rev. D **83**, 103514 (2011).
[60] P. J. Fox, G. D. Kribs, and T. M. Tait, Interpreting dark matter direct detection independently of the local velocity and density distribution, Phys. Rev. D **83**, 034007 (2011).
[61] M. T. Frandsen, F. Kahlhoefer, C. McCabe, S. Sarkar, and K. Schmidt-Hoberg, Resolving astrophysical uncertainties in dark matter direct detection, J. Cosmol. Astropart. Phys. 01 (2012) 024.
[62] J. Herrero-Garcia, T. Schwetz, and J. Zupan, Astrophysics Independent Bounds on the Annual Modulation of Dark Matter Signals, Phys. Rev. Lett. **109**, 141301 (2012).
[63] P. Gondolo and G. B. Gelmini, Halo independent comparison of direct dark matter detection data, J. Cosmol. Astropart. Phys. 12 (2012) 015.
[64] P. J. Fox, Y. Kahn, and M. McCullough, Taking halo-independent dark matter methods out of the bin, J. Cosmol. Astropart. Phys. 10 (2014) 076.
[65] S. D. McDermott, H.-B. Yu, and K. M. Zurek, The dark matter inverse problem: Extracting particle physics from scattering events, Phys. Rev. D **85**, 123507 (2012).
[66] A. H. G. Peter, V. Gluscevic, A. M. Green, B. J. Kavanagh, and S. K. Lee, WIMP physics with ensembles of direct-detection experiments, Phys. Dark Univ. **5–6**, 45 (2014).
[67] V. Gluscevic and A. H. G. Peter, Understanding WIMP-baryon interactions with direct detection: A roadmap, J. Cosmol. Astropart. Phys. 09 (2014) 040.
[68] J. D. Wells, Implications of supersymmetry breaking with a little hierarchy between gauginos and scalars, arXiv:hep-ph/0306127.
[69] N. Arkani-Hamed and S. Dimopoulos, Supersymmetric unification without low energy supersymmetry and signatures for fine-tuning at the LHC, J. High Energy Phys. 06 (2005) 073.
[70] G. Giudice and A. Romanino, Split supersymmetry, Nucl. Phys. **B699**, 65 (2004).
[71] J. D. Wells, PeV-scale supersymmetry, Phys. Rev. D **71**, 015013 (2005).
[72] W. Kilian, T. Plehn, P. Richardson, and E. Schmidt, Split supersymmetry at colliders, Eur. Phys. J. C **39**, 229 (2005).
[73] A. Arvanitaki, N. Craig, S. Dimopoulos, and G. Villadoro, Mini-split, J. High Energy Phys. 02 (2013) 126.
[74] L. J. Hall, Y. Nomura, and S. Shirai, Spread supersymmetry with wino LSP: Gluino and dark matter signals, J. High Energy Phys. 01 (2013) 036.
[75] J. Unwin, R-symmetric high scale supersymmetry, Phys. Rev. D **86**, 095002 (2012).
[76] Y. Kahn, M. McCullough, and J. Thaler, Auxiliary gauge mediation: A new route to mini-split supersymmetry, J. High Energy Phys. 11 (2013) 161.
[77] X. Lu, H. Murayama, J. T. Ruderman, and K. Tobioka, A Natural Higgs Mass in Supersymmetry from Nondecoupling Effects, Phys. Rev. Lett. **112**, 191803 (2014).
[78] P. J. Fox, G. D. Kribs, and A. Martin, Split dirac supersymmetry: An ultraviolet completion of Higgsino dark matter, Phys. Rev. D **90**, 075006 (2014).
[79] N. Nagata and S. Shirai, Higgsino dark matter in high-scale supersymmetry, J. High Energy Phys. 01 (2015) 029.
[80] Y. Nomura and S. Shirai, Supersymmetry from Typicality: TeV-Scale Gauginos and PeV-Scale Squarks and Sleptons, Phys. Rev. Lett. **113**, 111801 (2014).
[81] C. Cheung, L. J. Hall, D. Pinner, and J. T. Ruderman, Prospects and blind spots for neutralino dark matter, J. High Energy Phys. 05 (2013) 100.
[82] T. Han, Z. Liu, and A. Natarajan, Dark matter and Higgs bosons in the MSSM, J. High Energy Phys. 11 (2013) 008.
[83] C. Cheung and D. Sanford, Simplified models of mixed dark matter, J. Cosmol. Astropart. Phys. 02 (2014) 011.
[84] P. Huang and C. E. M. Wagner, Blind spots for neutralino dark matter in the MSSM with an intermediate m_A, Phys. Rev. D **90**, 015018 (2014).
[85] T. Han, Z. Liu, and S. Su, Light neutralino dark matter: Direct/indirect detection and collider searches, J. High Energy Phys. 08 (2014) 093.
[86] F. Yu, Di-jet resonances at future hadron colliders: A Snowmass whitepaper, arXiv:1308.1077.
[87] J. Anderson, Excited quark production at a 100 TeV VLHC, arXiv:1309.0845.
[88] T. Cohen, T. Golling, M. Hance, A. Henrichs, K. Howe, J. Loyal, S. Padhi, and J. G. Wacker, SUSY simplified models at 14, 33, and 100 TeV proton colliders, J. High Energy Phys. 04 (2014) 117.
[89] D. Curtin, P. Meade, and C.-T. Yu, Testing electroweak baryogenesis with future colliders, J. High Energy Phys. 11 (2014) 127.
[90] A. Fowlie and M. Raidal, Prospects for constrained supersymmetry at $\sqrt{s} = 33$ TeV and $\sqrt{s} = 100$ TeV

proton-proton super-colliders, Eur. Phys. J. C **74**, 2948 (2014).
[91] T. G. Rizzo, Fun with new gauge bosons at 100 TeV, Phys. Rev. D **89**, 095022 (2014).
[92] A. J. Larkoski and J. Thaler, Aspects of jets at 100 TeV, Phys. Rev. D **90**, 034010 (2014).
[93] A. Hook and A. Katz, Unbroken $SU(2)$ at a 100 TeV collider, J. High Energy Phys. 09 (2014) 175.
[94] A. J. Barr, M. J. Dolan, C. Englert, D. E. F. de Lima, and M. Spannowsky, Higgs self-coupling measurements at a 100 TeV hadron collider, J. High Energy Phys. 02 (2015) 016.
[95] M. Low and L.-T. Wang, Neutralino dark matter at 14 TeV and 100 TeV, J. High Energy Phys. 08 (2014) 161.
[96] T. Cohen, R. T. D'Agnolo, M. Hance, H. K. Lou, and J. G. Wacker, Boosting stop searches with a 100 TeV proton collider, J. High Energy Phys. 11 (2014) 021.
[97] M. Cirelli, F. Sala, and M. Taoso, Wino-like minimal dark matter and future colliders, J. High Energy Phys. 10 (2014) 033; 01 (2014) 041(E).
[98] B. S. Acharya, K. Bozek, C. Pongkitivanichkul, and K. Sakurai, Prospects for observing charginos and neutralinos at a 100 TeV proton-proton collider, arXiv:1410.1532.
[99] S. Gori, S. Jung, L.-T. Wang, and J. D. Wells, Prospects for electroweakino discovery at a 100 TeV hadron collider, J. High Energy Phys. 12 (2014) 108.
[100] D. Curtin, R. Essig, S. Gori, and J. Shelton, Illuminating dark photons with high-energy colliders, arXiv:1412.0018.
[101] G. G. di Cortona, Hunting electroweakinos at future hadron colliders and direct detection experiments, arXiv:1412.5952.
[102] G.-C. Cho, K. Hagiwara, J. Kanzaki, T. Plehn, D. Rainwater, and T. Stelzer, Weak boson fusion production of supersymmetric particles at the CERN LHC, Phys. Rev. D **73**, 054002 (2006).
[103] A. Djouadi, J.-L. Kneur, and G. Moultaka, SuSpect: A FORTRAN code for the supersymmetric and Higgs particle spectrum in the MSSM, Comput. Phys. Commun. **176**, 426 (2007).
[104] G. Belanger, F. Boudjema, A. Pukhov, and A. Semenov, micrOMEGAs3: A program for calculating dark matter observables, Comput. Phys. Commun. **185**, 960 (2014).
[105] D. M. Pierce, J. A. Bagger, K. T. Matchev, and R.-j. Zhang, Precision corrections in the minimal supersymmetric standard model, Nucl. Phys. **B491**, 3 (1997).
[106] T. Fritzsche and W. Hollik, Complete one loop corrections to the mass spectrum of charginos and neutralinos in the MSSM, Eur. Phys. J. C **24**, 619 (2002).
[107] W. Oller, H. Eberl, W. Majerotto, and C. Weber, Analysis of the chargino and neutralino mass parameters at one loop level, Eur. Phys. J. C **29**, 563 (2003).
[108] J. Hisano, S. Matsumoto, M. Nagai, O. Saito, and M. Senami, Non-perturbative effect on thermal relic abundance of dark matter, Phys. Lett. B **646**, 34 (2007).
[109] M. Cirelli, A. Strumia, and M. Tamburini, Cosmology and astrophysics of minimal dark matter, Nucl. Phys. **B787**, 152 (2007).
[110] A. Hryczuk, R. Iengo, and P. Ullio, Relic densities including Sommerfeld enhancements in the MSSM, J. High Energy Phys. 03 (2011) 069.
[111] A. Hryczuk and R. Iengo, The one-loop and Sommerfeld electroweak corrections to the wino dark matter annihilation, J. High Energy Phys. 01 (2012) 163.
[112] M. Beneke, C. Hellmann, and P. Ruiz-Femenia, Non-relativistic pair annihilation of nearly mass degenerate neutralinos and charginos III. Computation of the Sommerfeld enhancements, arXiv:1411.6924.
[113] M. Beneke, C. Hellmann, and P. Ruiz-Femenia, Heavy neutralino relic abundance with Sommerfeld enhancements—A study of pMSSM scenarios, arXiv:1411.6930.
[114] P. Ciafaloni, D. Comelli, A. De Simone, E. Morgante, A. Riotto, and A. Urbano*et al.*, The role of electroweak corrections for the dark matter relic abundance, J. Cosmol. Astropart. Phys. 10 (2013) 031.
[115] W. Beenakker, M. Klasen, M. Kramer, T. Plehn, M. Spira, and P. Zerwas, Production of Charginos, Neutralinos, and Sleptons at Hadron Colliders, Phys. Rev. Lett. **83**, 3780 (1999).
[116] S. Chatrchyan *et al.* (CMS Collaboration), Search for physics beyond the standard model in events with τ leptons, jets, and large transverse momentum imbalance in pp collisions at $\sqrt{s} = 7$ TeV, Eur. Phys. J. C **73**, 2493 (2013).
[117] S. Chatrchyan *et al.* (CMS Collaboration), Search for anomalous production of events with three or more leptons in pp collisions at $\sqrt{(}s) = 8$ TeV, Phys. Rev. D **90**, 032006 (2014).
[118] G. Aad *et al.* (ATLAS Collaboration), Search for direct production of charginos and neutralinos in events with three leptons and missing transverse momentum in $\sqrt{s} =$ 8 TeV pp collisions with the ATLAS detector, J. High Energy Phys. 04 (2014) 169.
[119] G. Aad *et al.* (ATLAS Collaboration), Search for the direct production of charginos, neutralinos and staus in final states with at least two hadronically decaying taus and missing transverse momentum in pp collisions at $\sqrt{s} =$ 8 TeV with the ATLAS detector, J. High Energy Phys. 10 (2014) 96.
[120] L. Calibbi, J. M. Lindert, T. Ota, and Y. Takanishi, Cornering light neutralino dark matter at the LHC, J. High Energy Phys. 10 (2013) 132.
[121] L. Calibbi, J. M. Lindert, T. Ota, and Y. Takanishi, LHC tests of light neutralino dark matter without light sfermions, J. High Energy Phys. 11 (2014) 106.
[122] G. F. Giudice, T. Han, K. Wang, and L.-T. Wang, Nearly degenerate gauginos and dark matter at the LHC, Phys. Rev. D **81**, 115011 (2010).
[123] S. Gori, S. Jung, and L.-T. Wang, Cornering electroweakinos at the LHC, J. High Energy Phys. 10 (2013) 191.
[124] P. Schwaller and J. Zurita, Compressed electroweakino spectra at the LHC, J. High Energy Phys. 03 (2014) 060.
[125] Z. Han, G. D. Kribs, A. Martin, and A. Menon, Hunting quasidegenerate Higgsinos, Phys. Rev. D **89**, 075007 (2014).
[126] H. Baer, A. Mustafayev, and X. Tata, Monojet plus soft dilepton signal from light higgsino pair production at LHC14, Phys. Rev. D **90**, 115007 (2014).

[127] C. Han, Probing light bino and higgsinos at the LHC, arXiv:1409.7000.
[128] J. Alwall, R. Frederix, S. Frixione, V. Hirschi, F. Maltoni, O. Mattelaer, H.-S. Shao, T. Stelzer, P. Torrielli, and M. Zaro, The automated computation of tree-level and next-to-leading order differential cross sections, and their matching to parton shower simulations, J. High Energy Phys. 07 (2014) 079.
[129] T. Sjostrand, S. Mrenna, and P. Z. Skands, PYTHIA 6.4 physics and manual, J. High Energy Phys. 05 (2006) 026.
[130] M. Cacciari, G. P. Salam, and G. Soyez, The anti-k_t jet clustering algorithm, J. High Energy Phys. 04 (2008) 063.
[131] M. Cacciari, G. P. Salam, and G. Soyez, FastJet user manual, Eur. Phys. J. C **72**, 1896 (2012).
[132] J. de Favereau, C. Delaere, P. Demin, A. Giammanco, V. Lemaître, A. Mertens, and M. Selvaggi, DELPHES 3, A modular framework for fast simulation of a generic collider experiment, J. High Energy Phys. 02 (2014) 057.
[133] J. Anderson, A. Avetisyan, R. Brock, S. Chekanov, T. Cohen *et al.*, Snowmass energy frontier simulations, arXiv:1309.1057.
[134] G. Cullen, N. Greiner, and G. Heinrich, Susy-QCD corrections to neutralino pair production in association with a jet, Eur. Phys. J. C **73**, 2388 (2013).
[135] B. Fuks, M. Klasen, D. R. Lamprea, and M. Rothering, Gaugino production in proton-proton collisions at a center-of-mass energy of 8 TeV, J. High Energy Phys. 10 (2012) 081.
[136] J. Debove, B. Fuks, and M. Klasen, Transverse-momentum resummation for gaugino-pair production at hadron colliders, Phys. Lett. B **688**, 208 (2010).
[137] J. Debove, B. Fuks, and M. Klasen, Joint resummation for gaugino pair production at hadron colliders, Nucl. Phys. **B849**, 64 (2011).
[138] G. Aad *et al.* (ATLAS Collaboration), Report No. ATL-PHYS-PUB-2011-007, 2011.
[139] M. Ibe, S. Matsumoto, and R. Sato, Mass splitting between charged and neutral winos at two-loop level, Phys. Lett. B **721**, 252 (2013).
[140] J. Bramante, A. Delgado, F. Elahi, A. Martin, and B. Ostdiek, Catching sparks from well-forged neutralinos, Phys. Rev. D **90**, 095008 (2014).
[141] C. Han, L. Wu, J. M. Yang, M. Zhang, and Y. Zhang, A new approach for detecting compressed bino/wino at the LHC, arXiv:1409.4533.
[142] T. Sjostrand, S. Mrenna, and P. Z. Skands, A brief introduction to PYTHIA 8.1, Comput. Phys. Commun. **178**, 852 (2008).